

A Broadband High-Gain Fabry-Perot Cavity Antenna for Vehicle-to-Everything Applications

Mia Maria Ulfah¹, Panuwat Janpugdee¹, Danai Torrungrueng², and Hsi-Tseng Chou³

¹Chulalongkorn University

²King Mongkut's University of Technology North Bangkok

³Graduate Institute of Communication Engineering, National Taiwan University

March 05, 2024

Abstract

In this paper, a Fabry-Perot cavity (FPC) antenna with a partially reflective surface (PRS) consisting of two dielectric slabs with identical thickness and permittivity to increase the gain with wide bandwidth is presented. The PRS is placed in front of a broadband U-shaped microstrip patch antenna to create an air-filled cavity between the PRS and the ground plane of the antenna structure. The configuration of the two dielectric slabs aims to create a positive phase gradient of the reflection coefficient, which strongly controls the gain bandwidth performance. The proposed PRS was first designed and analyzed using a transmission line model and then verified by a full-wave simulation. The measurement results show that the proposed FPC antenna achieves a gain improvement of up to 5 dB compared to the antenna without PRS, with a 3-dB gain bandwidth of 11.5% and a broadside peak gain of 9.88 dBi. In addition, the measured impedance bandwidth is approximately 18.8% and ranges from 4.95–6 GHz, which covers the required frequency band for vehicle-to-everything (V2X) applications.

20 **Abstract**

21 In this paper, a Fabry-Perot cavity (FPC) antenna with a partially reflective surface (PRS)
22 consisting of two dielectric slabs with identical thickness and permittivity to increase the gain with
23 wide bandwidth is presented. The PRS is placed in front of a broadband U-shaped microstrip patch
24 antenna to create an air-filled cavity between the PRS and the ground plane of the antenna
25 structure. The configuration of the two dielectric slabs aims to create a positive phase gradient of
26 the reflection coefficient, which strongly controls the gain bandwidth performance. The proposed
27 PRS was first designed and analyzed using a transmission line model and then verified by a full-
28 wave simulation. The measurement results show that the proposed FPC antenna achieves a gain
29 improvement of up to 5 dB compared to the antenna without PRS, with a 3-dB gain bandwidth of
30 11.5% and a broadside peak gain of 9.88 dBi. In addition, the measured impedance bandwidth is
31 approximately 18.8% and ranges from 4.95–6 GHz, which covers the required frequency band for
32 vehicle-to-everything (V2X) applications.

33 **Plain Language Summary**

34 A new design of a broadband antenna with high gain has been developed by using two identical
35 dielectric slabs placed in front of a broadband microstrip patch. This antenna is intended for
36 vehicle-to-everything (V2X) communications. The proposed configuration increases the degrees
37 of freedom and design flexibility to improve the antenna gain over a wide frequency range. The
38 proposed antenna is more practical as it is compact, lightweight, and easy to fabricate.

39 **1 Introduction**

40 The popularity of smart transportation has led to the development of vehicular wireless
41 communication systems, with vehicle-to-everything (V2X) emerging as a significant development
42 in enhancing connectivity and communication capabilities within the advancement of
43 transportation technology. In conjunction with the advanced driver assistant system (ADAS), V2X
44 will enhance safety as well as situational awareness, optimizing traffic efficiency, and overall
45 transportation effectiveness. There are two different standards for V2X communications, namely
46 the WLAN-based standard and the cellular-based standard. The WLAN-based standard refers to
47 IEEE 802.11p designed specifically for V2X communications operating in the 5 GHz band, while
48 for the cellular-based standard, e.g., cellular vehicle-to-everything (C-V2X) operating at the
49 frequency of 5.9 GHz.

50 A highly directive antenna is required to provide high antenna gain for strong signal
51 strength, a longer communication range, higher reliability, and better resistance to interference.
52 These features are essential to ensure reliable communication between vehicles and infrastructure
53 for safety enhancement. However, conventional high-gain antennas, such as reflectors, Yagi-Uda,
54 and array antennas, possess large and complex physical configurations and are thus unsuitable for
55 vehicular applications. Recently, the Fabry-Perot cavity (FPC) antennas garnered the attention of
56 many researchers due to their good characteristics, such as high efficiency, high gain, and simple
57 feeding technique. The concept of FPC antennas was first proposed in 1956 (Trentini, 1956), where
58 a PRS is placed in front of the source or feed antenna with a ground plane. The PRS is positioned
59 at a certain distance from the ground plane of the source antenna to create an air cavity in between.
60 The electromagnetic (EM) waves produced by the radiating antenna will undergo multiple
61 reflections within the cavity. This process results in an in-phase superposition of associated EM
62 waves if the resonant conditions are satisfied. Consequently, highly directive radiation is formed.

63 The conventional design of FPC has a narrow gain bandwidth (BW) because of its resonant
 64 characteristics. Several approaches have been proposed to broaden the gain BW. A single-layer
 65 unprinted dielectric substrate with a transverse permittivity gradient (TPG) was used to overcome
 66 the bandwidth limitation (Hashmi & Esselle, 2016; Baba, Hashmi, & Esselle, 2017). In Ji, Qin, &
 67 Guo (2017), by utilizing a flat ground plane at the center and angularly tilting it upwards in a
 68 trapezoid shape at the corner, the 3-dB gain bandwidth of the proposed antenna has been increased
 69 to 20.2%. These methods effectively improve the gain BW but suffer from complex design and
 70 fabrication processes. Another common technique uses a PRS with a positive phase gradient. This
 71 type of response can be obtained using a frequency-selective surface (FSS), which can be classified
 72 as a printed PRS. Two-layer PRSs consisting of hexagonal and tripod branch unit cells were
 73 employed for size reduction and to make the FPC antenna more compact, achieving a peak gain
 74 of 14.2 dBi and 3-dB gain BW of 34.2% (Guan et al., 2021). Using two types of FSS unit cells
 75 arranged in a chessboard pattern on a single-layer substrate to create a hybrid PRS (HPRS) was
 76 reported (Liu et al., 2020). The hybrid surface (HS) and reflective surface (RS) are formed by
 77 employing cross and square ring-shaped patches, which results in a measured peak gain of 17.08
 78 dBi and a 3-dB gain BW of 25.4%. A complementary unit cell design was also proposed to provide
 79 a positive phase gradient (Wang et al., 2014; Lian, Tang & Yin, 2018; Meriche et al., 2019).
 80 Subsequently, multilayer dielectric slabs, classified as unprinted PRSs, were also used to obtain a
 81 positive phase gradient (Zeb et al., 2012; Al-Tarifi et al., 2013; Wang et al., 2015). A combination
 82 of multiple thin dielectric slabs arranged closely together was reported (Nguyen-Trong et al.,
 83 2018). The thicknesses are only $0.1\lambda_{\text{subs}}$ (λ_{subs} is the dielectric wavelength at the center
 84 frequency). These slabs were separated by a $0.1\lambda_0$ (λ_0 is the free space wavelength) air gap. The
 85 measured maximum gain is 14.2 dBi, and the 3-dB gain bandwidth is up to 86%.

86 The aforementioned literature has demonstrated that the unprinted PRS exhibits superior
 87 performance in terms of gain BW enhancement despite its simple structure. Taking the potential
 88 of unprinted PRSs in gain enhancement, a broadband and high-gain FPC antenna presented in this
 89 paper is intended to work for V2X communications. The antenna configuration consists of PRSs
 90 placed over a broadband microstrip patch antenna. The proposed PRS consists of two dielectric
 91 substrate slabs with an equal thickness and dielectric constant; they are separated by an air cavity.
 92 The PRS reflection coefficient with a positive phase gradient improves gain performance over a
 93 wide frequency range.

94 The rest of this paper is organized as follows. Section 2 presents the design and analysis of
 95 the PRS. The antenna design and simulation results are illustrated in Section 3. In Section 4, the
 96 measurement results are shown, and the proposed work is compared with some competing designs
 97 in the literature. Finally, conclusions are provided in Section 5.

98 2 PRS Design and Analysis

99 A PRS is a surface that reflects part of the incident EM waves while transmitting the rest.
 100 In antenna applications, the PRS is placed in front of the feed antenna to control the radiated EM
 101 wave and improve the radiation performance of the antenna. The properties of PRSs have a strong
 102 influence on the radiation characteristics of the antenna, such as gain, radiation pattern, and
 103 operating BW. The PRS and the ground plane, which is usually part of the feed antenna, form an
 104 air cavity in which multiple reflections of EM waves occur. The mechanism for improving the
 105 antenna gain is based on the resonance of the EM waves in the cavity. The most important property
 106 of the PRS is its complex reflection coefficient ($\Gamma_{PRS} = |\Gamma_{PRS}| e^{j\phi_{PRS}}$). The reflection phase

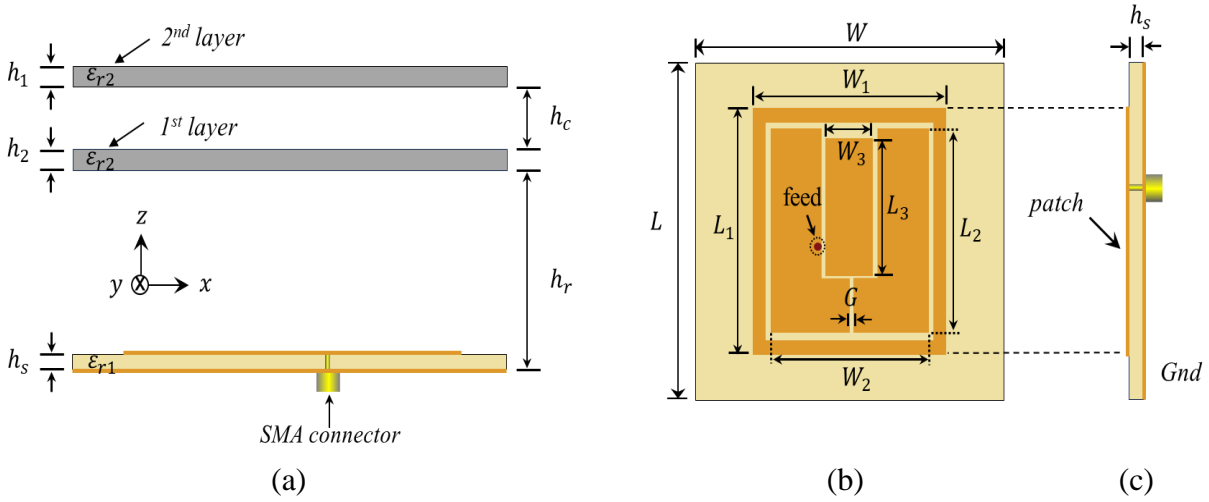


Figure 1. Design of the proposed antenna. (a) cross-section view (b) top-view of feed antenna (c) side-view of feed antenna.

107 (ϕ_{PRS}), or the phase of the reflection coefficient, of the PRS for a resonant condition of the cavity
 108 in the broadside direction of the antenna (perpendicular to the PRS) can be expressed as follows
 109 (Trentini, 1956):

$$\phi_{PRS} = \frac{4\pi h_r}{\lambda_0} + 2N\pi + \phi_{GND}, \quad (1)$$

110 where $N = 0, \pm 1, \pm 2, \dots$, ϕ_{GND} is the phase of the reflection coefficient of the ground plane, and
 111 h_r is the height of the air cavity between the PRS and the ground plane. From (1) it can be seen
 112 that a positive phase gradient of the PRS reflection coefficient over a wide frequency range is
 113 required to achieve a wide gain BW of the FPC antenna.

114 The PRS structure can consist of a variety of materials, including dielectrics, metals, or
 115 combinations thereof. One of the simplest PRS structures consists only of dielectric substrates
 116 (unprinted PRS). The functional mechanism of the PRS can be described using analytical methods
 117 such as the transmission line (TL) model. Using the TL model can show that a single-layer
 118 dielectric PRS should be half a wavelength thick to achieve the desired reflection phase
 119 characteristics (Nguyen-Trong et al., 2018). However, opting for this thickness leads to an
 120 unwieldy antenna. In addition, the desired thickness of substrate for the operating frequency range
 121 may not be commercially available.

122 The configuration of the FPC antenna presented in this work is shown in Figure 1. The
 123 proposed PRS consists of two layers of dielectric substrates with the same thickness ($h_1 = h_2$) and
 124 dielectric constant (ϵ_{r2}), separated by an air gap (h_c). The use of a two-layer PRS leads to more
 125 degrees of freedom and offers more flexibility in the design process. Several variables can be
 126 varied to achieve the desired reflection properties of the PRS, i.e., the dielectric constant and the
 127 thickness of the substrate as well as the height of the air gap. Given the unavailability of a particular
 128 material thickness in the market, modifying the air cavity height will be more convenient than
 129 altering the substrate thickness.

130 The two dielectric substrates used in the present design are Rogers RT/duroid 6010LM
 131 ($\epsilon_r = 10.2$) with a thickness of 1.9 mm ($0.11\lambda_g$), where λ_g is the wavelength in the substrate at the

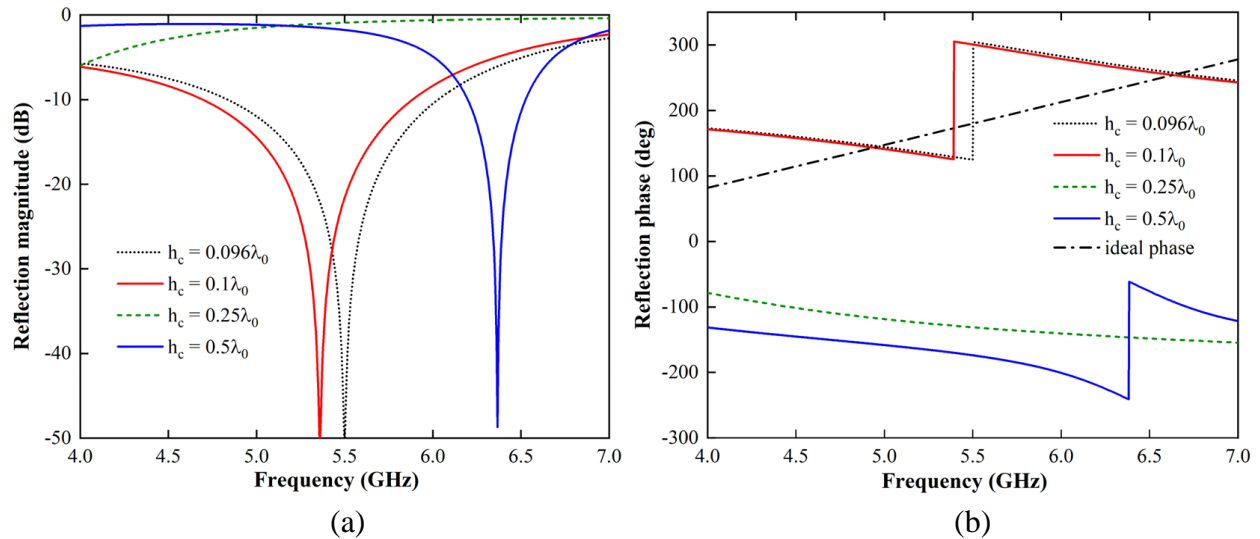


Figure 2. Reflection coefficients of the proposed PRS with different heights of the air gap calculated with the TL model. (a) magnitude (b) phase.

132 center frequency. The height of the air gap (h_c) is properly chosen to obtain a positive phase
 133 gradient. Figure 2 shows the reflection coefficients calculated with the TL model for the proposed
 134 PRS with different heights of the air gap. Also shown is a plot of the ideal positive phase gradient,
 135 which intersects with the plots of the reflection coefficient phase. It can be seen that the positive
 136 phase gradient intersects with the ideal phase at the resonant frequency when the height of the air
 137 gap is set to $0.096\lambda_0$ (5.17 mm).

138 To verify the preliminary design by the TL model, the proposed PRS structure is also
 139 simulated with CST Studio Suite (Dassault Systèmes, 2021). It is modeled as a periodic unit cell,
 140 as shown in Figure 3, to simplify the simulation. The magnitude and phase of the reflection
 141 coefficients obtained using CST Studio Suite and the TL model are compared in Figure 3. It can
 142 be seen that both results agree very well.

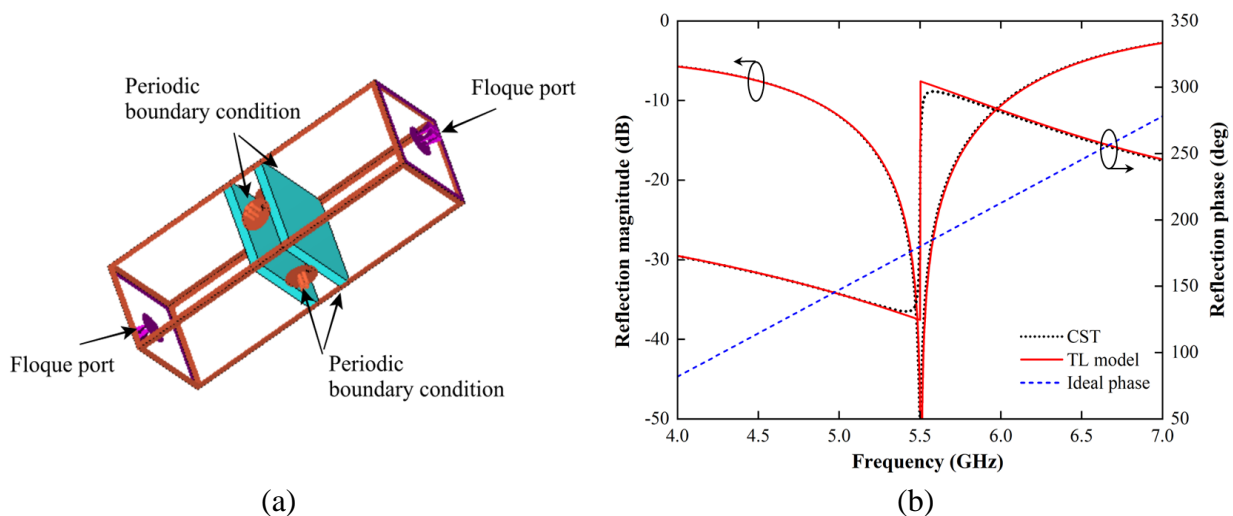


Figure 3. (a) Unit cell model of the proposed PRS in the simulation. (b) reflection coefficients of the proposed PRS determined by CST Studio Suite and the TL model.

143 It has been demonstrated in this section that by carefully choosing the thickness of the
 144 substrate and the air gap, the phase response can exhibit a positive gradient and intersect with the
 145 ideal phase given on the right-hand side (RHS) of (1) over a wide frequency band. Note that, with
 146 the proposed PRS, the positive phase gradient can be obtained with a more compact structure,
 147 namely $0.11\lambda_g + 0.095\lambda_0 + 0.11\lambda_g$.

148 3 Antenna Design and Characterization

149 The proposed FPC antenna configuration consists of two main parts: a feed antenna and
 150 the PRS. The feed antenna plays an important role in determining the performance of the designed
 151 antenna. The directivity of the feed antenna contributes to the achieved directivity of the FPC
 152 antenna as described by the following equation (Niaz et al., 2021):

$$D_{FPCA} = D_{feed} + D_{PRS}, \quad (2)$$

153 where D_{FPCA} is the directivity of FPC antenna, D_{feed} and D_{PRS} are the feed antenna and PRS
 154 directivities, respectively.

155 In this paper, the microstrip patch antenna is used as the feed antenna because it is known
 156 for its outstanding features such as low cost, low profile, planar structure, and easy fabrication.
 157 The microstrip patch antenna is printed on the FR-4 substrate ($\epsilon_{r1} = 4.3$) with a thickness (h_s) of
 158 1.6 mm. The 50-ohm coaxial probe is used to feed the antenna through the SMA connector. The
 159 design evolution of the microstrip antenna and their simulated reflection coefficient magnitude
 160 ($|S_{11}|$) results are given in Figure 4.

161 Note that Ant_1 consists of a U-shaped patch to obtain a wide impedance BW ($|S_{11}| \leq -10$
 162 dB). This antenna generates two resonant modes, namely TM_{20} (5 GHz) and TM_{21} (5.9 GHz). The
 163 introduction of a slot into the structure (Ant_2) causes the second resonance TM_{02} (5.7 GHz) to
 164 appear and is combined with a rectangular patch (Ant_3) placed in the center of the U-shaped
 165 patch. This configuration creates a multimode resonance, resulting in a wide impedance BW.
 166 Finally, Ant_4 is designed by adding the rectangular ring to further broaden the impedance BW.
 167 The final design of the microstrip antenna exhibits an impedance BW range from 4.969 to 6.001
 168 GHz (18.96%), aligning perfectly with the frequency band requirements for V2X applications.

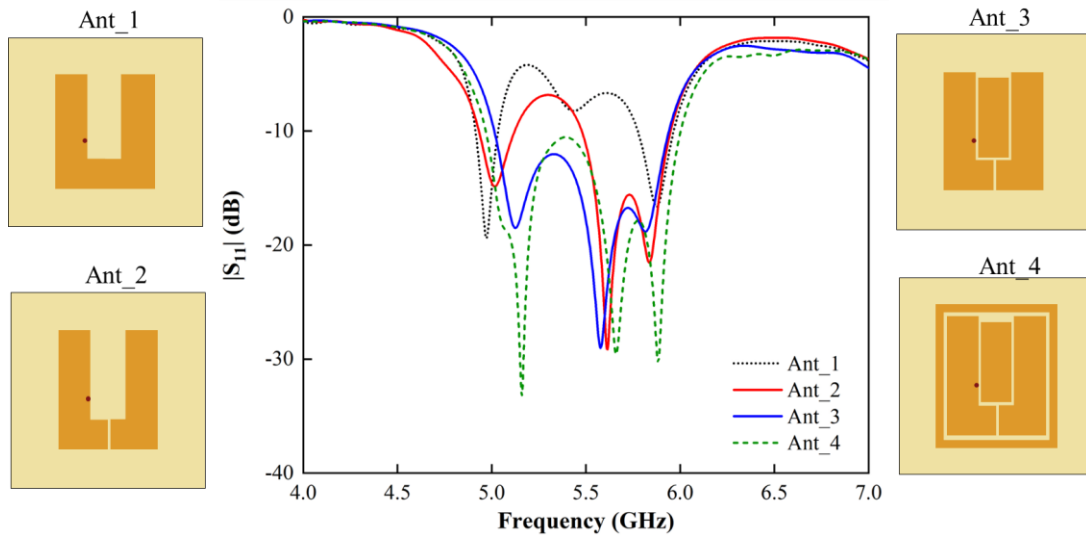


Figure 4. Geometry evolution of the microstrip antenna and its simulated $|S_{11}|$.

169 The designed PRS is then integrated into the feed antenna. The FPC is formed by the PRS
 170 and the ground plane of the feed antenna. The reflection phase of PRS is known from the
 171 simulation results, and the reflection coefficient of the ground plane (assuming PEC) is
 172 approximately -1 . Therefore, the height of the FPC between the PRS and the ground plane (h_r)
 173 can be determined using (1). With $\phi_{PRS} = 221.76^\circ$, $\phi_{GND} \approx 180^\circ$, and $N = 0$, $h_r = 30.44$ mm is
 174 obtained. However, to enhance the gain performance of the FPC antenna, the cavity height (h_r)
 175 was further optimized using CST Studio. Figure 5 shows the $|S_{11}|$ and broadside gain characteristics
 176 when h_r is varied. After the optimization, it is found that $h_r = 28.67$ mm is the optimum value.
 177 The geometric parameters of the proposed FPC antenna are listed in Table 1.

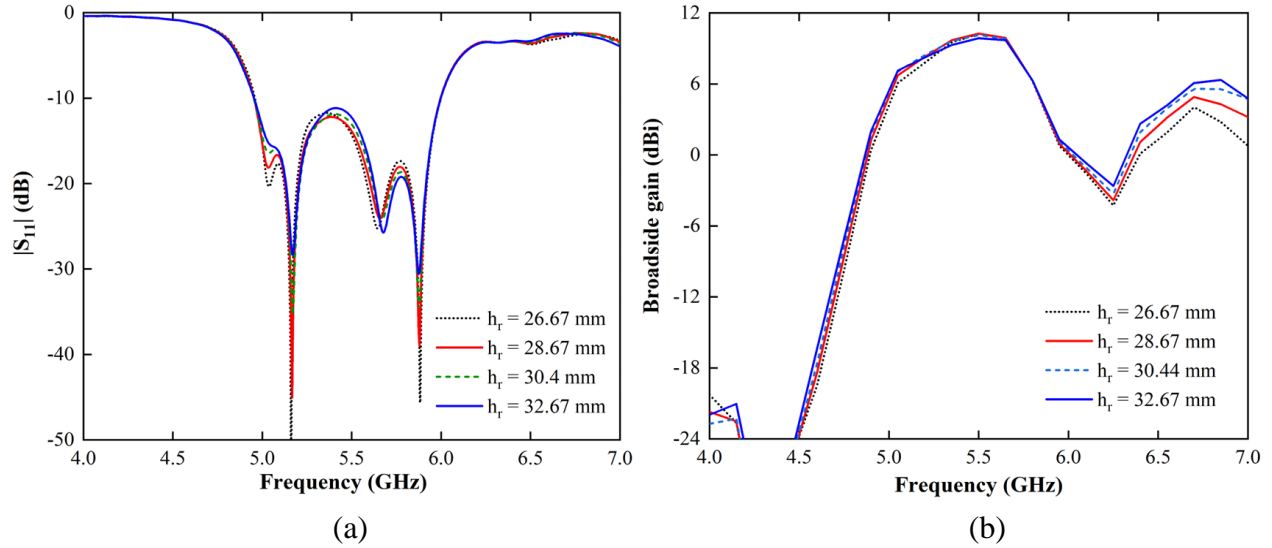


Figure 5. Performances of the proposed antenna with values of h_r varied. (a) simulated $|S_{11}|$ (b) simulated broadside gain.

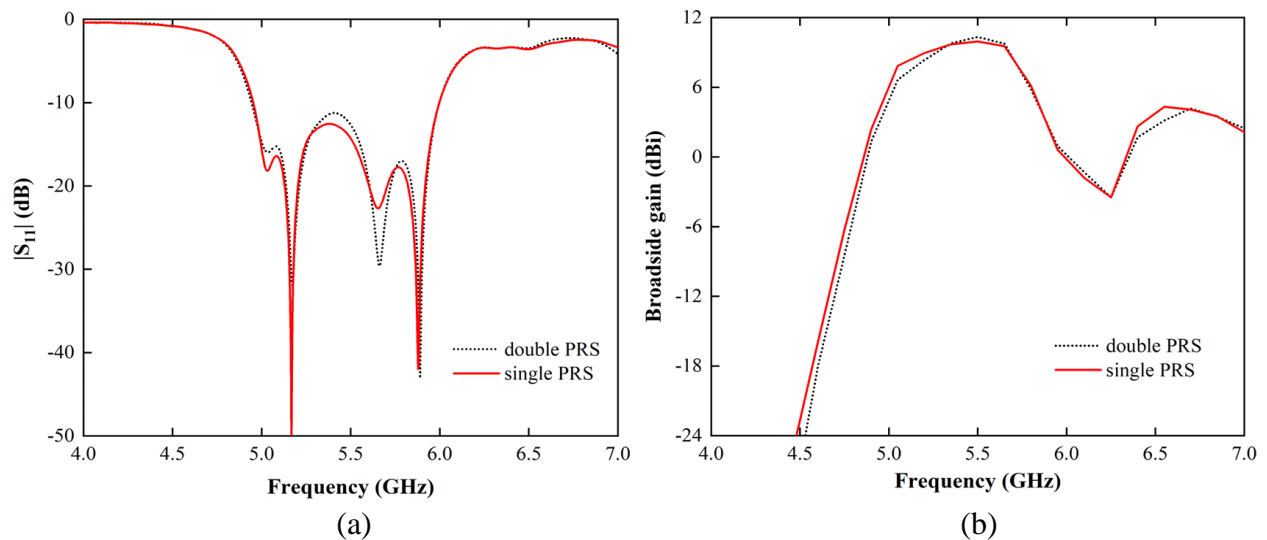


Figure 6. Comparison of the proposed antenna with single-layer PRS. (a) simulated $|S_{11}|$ (b) simulated broadside gain.

179

Table 1 Geometric Parameters of The Proposed FPC Antenna.

| Parameters | Values (mm) | Parameters | Values (mm) | Parameters | Values (mm) |
|------------|-------------|------------|-------------|------------|-------------|
| L | 60 | W_2 | 25 | h_1 | 1.9 |
| W | 60 | L_3 | 19.5 | h_2 | 1.9 |
| L_1 | 36 | W_3 | 8 | h_r | 28.67 |
| W_1 | 32 | G | 1 | h_c | 5.17 |
| L_2 | 28 | h_s | 1.6 | — | — |

180

181

182

183

184

A half-wavelength thickness of single-layer PRS is compared with the proposed double-layer PRS. The single-layer PRS has a thickness of 8.5 mm, whilst the proposed double-layer PRS has an overall thickness of 8.8 mm (including air gap). The thicknesses are almost equal. However, the proposed PRS is lighter. As seen, the performances of simulated $|S_{11}|$ and broadside gain are very similar to each other as plotted in Figure 6.

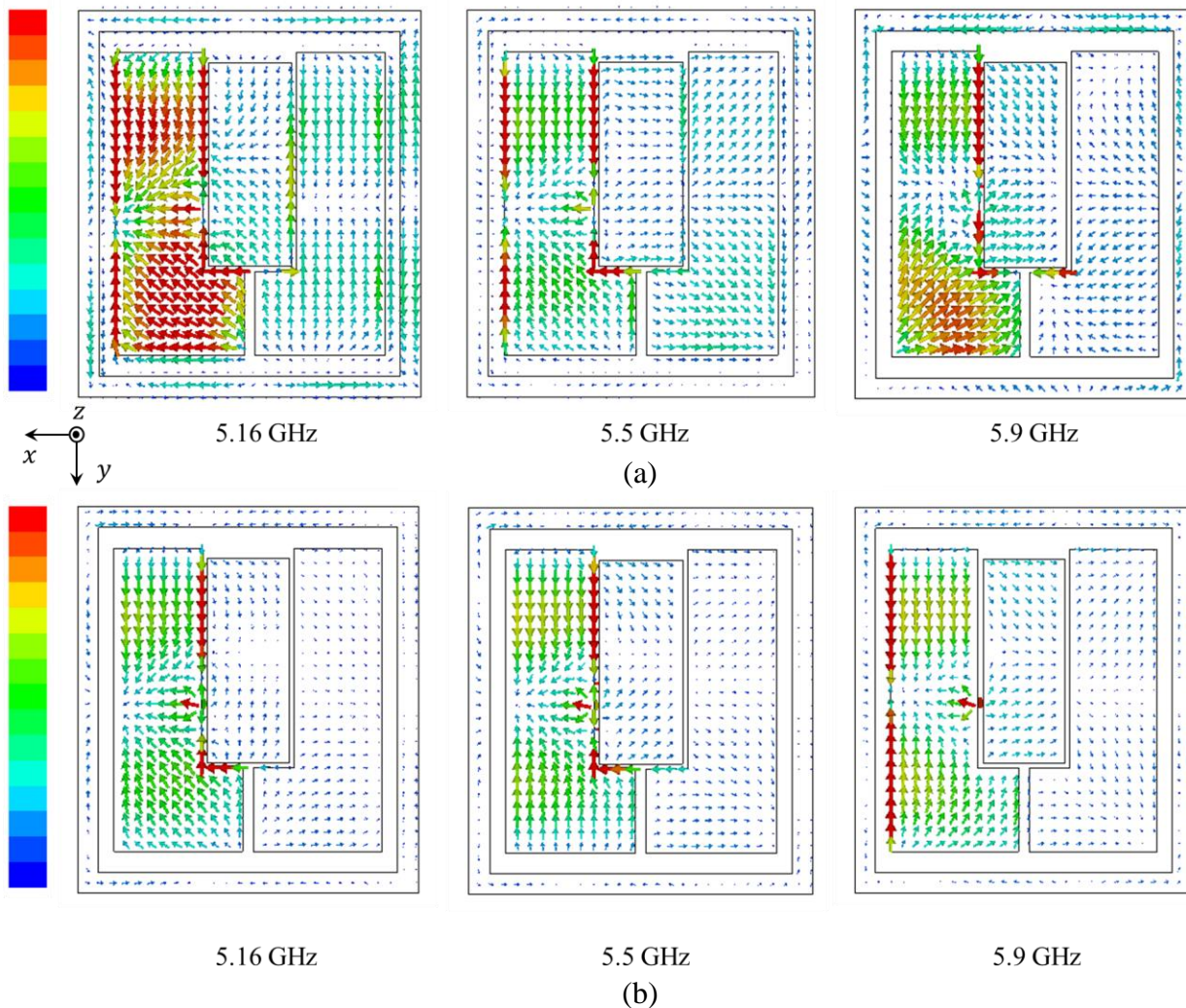


Figure 7. Surface current distribution at three resonant frequencies. (a) feed antenna (without the PRS) (b) feed antenna with the PRS.

185 Figure 7 shows the surface current distribution on the metallic portion of the antenna at
 186 three resonant frequencies. The introduction of the PRS in the feed antenna significantly affects
 187 the current distribution. The PRS can alter the EM environment around the antenna, leading to
 188 changes in the way current flows on the antenna structure. The reflective properties of the PRS
 189 affect the phase and amplitude of the EM waves, which in turn, can impact the impedance
 190 matching, radiation pattern, and overall performance of the feed antenna.

191 4 Results and Discussions

192 To validate the simulation results, the proposed FPC antenna is then fabricated where the
 193 prototype is given in Figure 8(a). The nylon is used to support the PRS layers and create an air
 194 cavity. The measurements were performed in an anechoic chamber as shown in Figure 8(b).

195 The comparison of simulated and measured $|S_{11}|$ is depicted in Figure 9(a), where the -10
 196 dB impedance BW for the feed antenna (without the PRS) is 18.82% (4.969–6.001 GHz), and
 197 18.64% (4.963–5.983 GHz) with respect to the center frequency, respectively. Additionally, it can
 198 be seen that the simulated -10 dB impedance BW for the antenna with PRS is 19.02%
 199 (4.954–5.995 GHz), and the measured one is 18.80% (4.95–5.977 GHz). In Figure 9(b), the
 200 presence of PRS significantly increases the broadside gain of the feed antenna from 4.85 to 9.88
 201 dBi, with a 3-dB gain BW of 11.5% in the measured result, while the simulated result is from 5.89
 202 to 10.32 dBi with 11.74% of 3-dB gain BW. Overall, the simulated and measured results are in
 203 good agreement. The slight discrepancies may be caused by fabrication errors, uncertainty of
 204 material properties, and soldering issues.

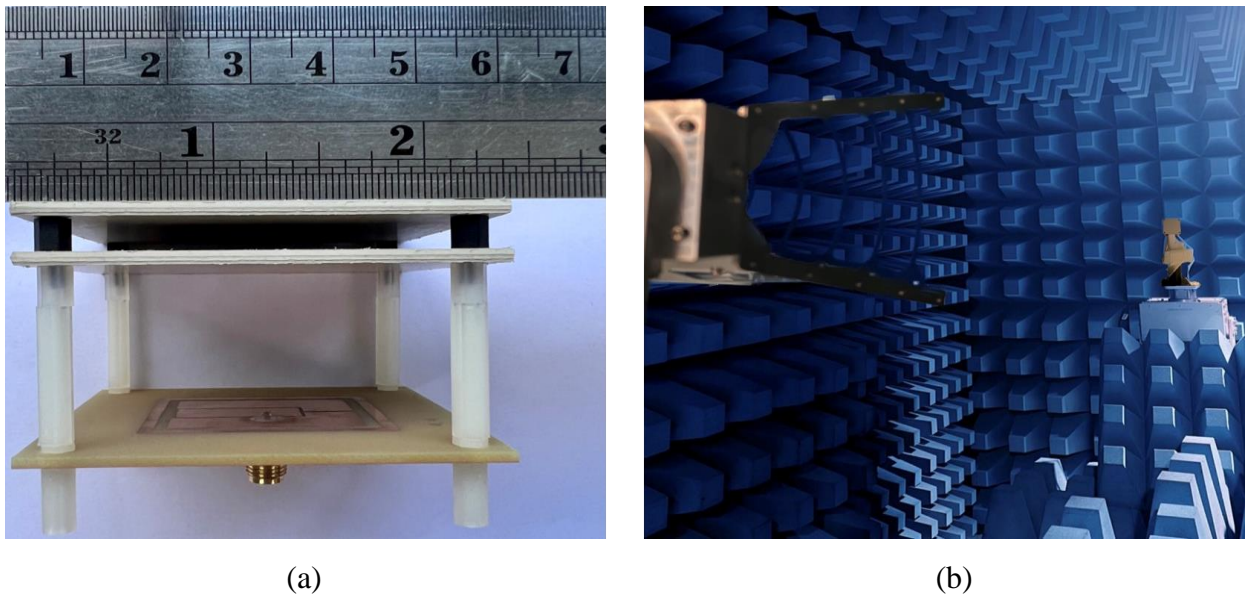


Figure 8. (a) Fabricated FPC antenna (b) radiation measurement set-up.

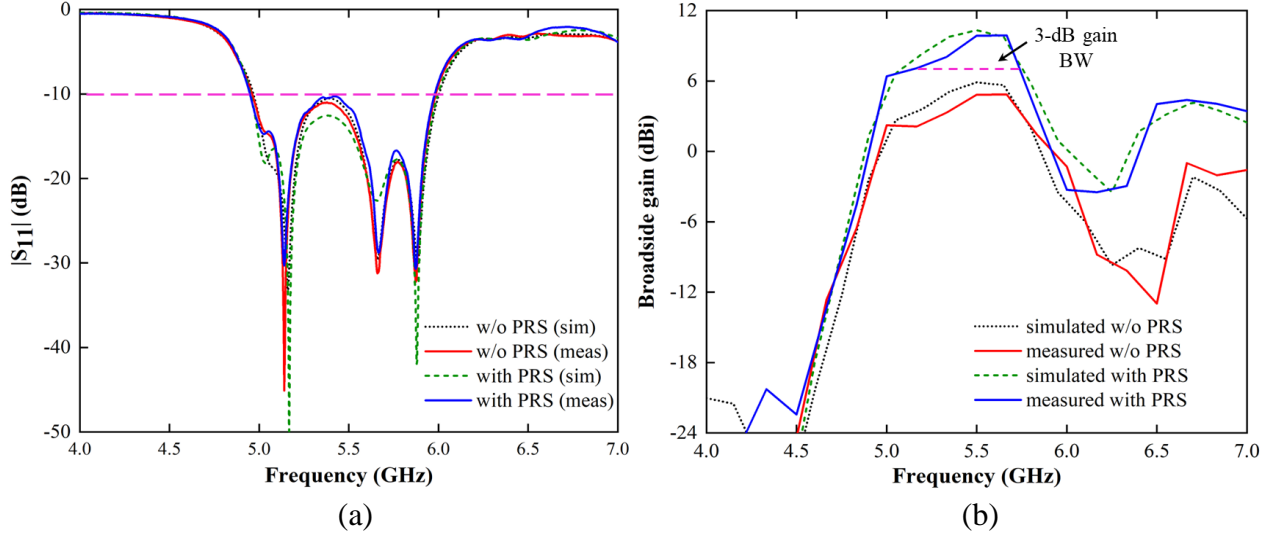


Figure 9. The comparison between simulated and measured results of the FPC antenna. (a) $|S_{11}|$ (b) broadside gain.

206 The simulated and measured radiation patterns of the proposed antenna at 5.16, 5.5, and
 207 5.9 GHz are plotted in Figure 10. It can be observed that the main beam orientation of the FPC
 208 antenna is in the broadside direction at three distinct frequencies in the H-plane, while at 5.9 GHz
 209 the main beam orientation is slightly tilted in the E-plane. It is noteworthy that since the antenna
 210 excitation is not symmetric in the E- and H-planes, the antenna has an asymmetric radiation
 211 pattern in both planes.

212 Table 2 compares the performance of the proposed FPC antenna with some previous works
 213 of vehicular antennas in the literature. It can be seen that the proposed antenna has a comparatively
 214 high gain and a fairly wide BW with a relatively compact size. It also has a simple structure with
 215 only a single feed and is easy to fabricate.

216 **Table 2** Comparison between the Proposed FPC Antenna and Reported Antennas.
 217

| References | f_{min} (GHz) | Size ($\lambda_{f_{min}}$ *) | IBW (%) | Max. gain (dBi) | 3-dB gain BW (%) | Num. of layers | Rad. pattern type |
|--------------------------|-----------------|--|--------------|-----------------|------------------|----------------|-------------------|
| (Sufian et al., 2022) | 5.61 | $1.38 \times 1.38 \times 0.03$ | 7.05 | 7.68 | N/A | 1 | Directional |
| (Xing et al., 2022) | 4.82 | $3.2 \times 2.41 \times 0.08$ | 27.6 | 4.2 | 7.8 | 1 | Directional |
| (Sun, Leung, & Lu, 2021) | 5.3 | $0.53 \times 0.35 \times 0.11$ | 41.6 | 8.46 | 10.3 | 2 | Directional |
| (Gao et al., 2018) | 5.42 | $3.07 \times 3.07 \times 0.08$ | 9.8 | 7.5 | N/A | 2 | Omni-directional |
| (Wong, So & Gao, 2016) | 4.82 | $1.03 \times 1.03 \times 0.05$ | 32.2 | 6.5 | 32.25 | 1 | Omni-directional |
| This work | 4.95 | $0.99 \times 0.99 \times 0.62$ | 18.80 | 9.88 | 11.5 | 3 | Directional |

218 * $\lambda_{f_{min}}$ is the free-space wavelength at the lowest frequency of the bandwidth.

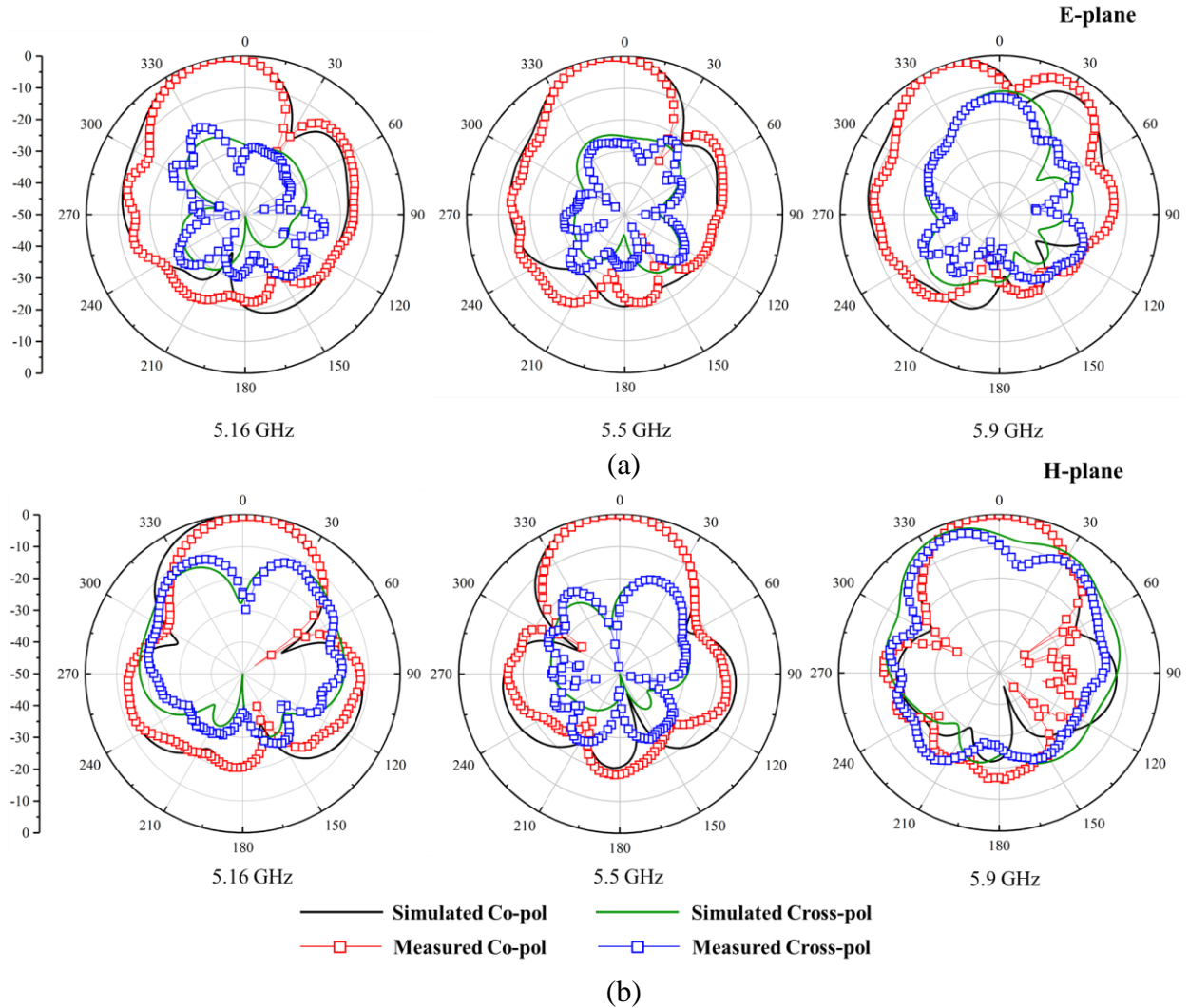


Figure 10. Simulated and measured radiation patterns of the FPC antenna at 5.16 GHz, 5.5 GHz, and 5.9 GHz. (a) E-plane (b) H-plane.

219 5 Conclusions

220 This paper presents a broadband high-gain FPC antenna for V2X communications. The
 221 gain-bandwidth performance is achieved through the appropriate design of the PRS reflection
 222 coefficient that exhibits a positive phase gradient. The proposed PRS is readily realized by two
 223 dielectric substrates with the same dielectric constant and thickness separated by an air gap with a
 224 suitable height. This structure is relatively practical since it is compact, lightweight, and easy to
 225 fabricate. The measurement results show that the proposed PRS can effectively increase the gain
 226 of the feed antenna with wide gain BW. In addition, a novel asymmetric PRS design based on
 227 compact microstrip resonant cells (CMRCs) is currently investigated for future works.
 228 Experimental characterizations of this novel PRS design are still in progress, where the
 229 measurement results will be reported later.

231 **Acknowledgments**

232 This research was funded in parts by (i) Ratchadapisek Somphot Fund for Wireless
233 Network & Future Internet Research Unit, Chulalongkorn University [Contract no. GRU
234 6409521015-1], (ii) National Science, Research and Innovation Fund (NSRF), King Mongkut's
235 University of Technology North Bangkok [Project no. KMUTNB-FF-67-A-04], and (iii) The
236 Ministry of Science and Technology, Taiwan.

237

238 **References**

- 239 Al-Tarifi, M. A., Anagnostou, D. E., Amert, A. K., & Whites, K. W. (2013). Bandwidth
240 enhancement of the resonant cavity antenna by using two dielectric superstrates. *IEEE*
241 *Transactions on Antennas and Propagation*, 61(4), 1898-1908. DOI: 10.1109/TAP.2012.2231931
- 242 Baba, A. A., Hasmi, R. M., & Esselle, K. P. (2017). Achieving a large gain-bandwidth product
243 from a compact antenna. *IEEE Transactions on Antennas and Propagation*, 65(7), 3437-3446.
244 DOI: 10.1109/TAP.2017.2700016
- 245 Dassault Systèmes. (2021). *CST Studio Suite 2021, Dassault Systèmes*. Retrieved from:
246 <https://www.3ds.com/products-services/simulia/products/cst-studio-suite/solvers/>
- 247 Gao, S., Ge, L., Zhang, D., & Qin, W. (2018). Low-profile dual-band stacked microstrip
248 monopolar patch antenna for WLAN and car-to-car communications. *IEEE Access*, 6,
249 69575-69581. DOI: 10.1109/ACCESS.2018.2877420
- 250 Guan, Y., Jiao, Y-C., Yan, Y-D., Feng, Y., Weng, Z., & Tian, J. (2021). Wideband and compact
251 Fabry-Perot resonator Antenna using partially reflective surfaces with regular hexagonal unit.
252 *IEEE Antennas and Wireless Propagation Letters*, 20(6), 1048-1052. DOI:
253 10.1109/LAWP.2021.3070376
- 254 Hashmi, R. M., & Esselle, K. P. (2016). A class of extremely wideband resonant cavity antennas
255 with large directivity-bandwidth products. *IEEE Transactions on Antennas and Propagation*,
256 64(2), 830-835. DOI: 10.1109/TAP.2015.2511801
- 257 Ji, L-Y., Qin, P-Y., & Guo, Y. J. (2018). Wideband Fabry-Perot cavity antenna with a shaped
258 ground plane. *IEEE Access*. 6. 2291-2297. DOI: 10.1109/ACCESS.2017.2782749
- 259 Lian, R., Tang, Z., & Yin, Y. (2018). Design of a broadband polarization-reconfigurable Fabry-
260 Perot resonator antenna. *IEEE Antennas and Wireless Propagation Letters*, 17(1), 122-125. DOI:
261 10.1109/LAWP.2017.2777502
- 262 Liu, Z., Liu, S., Zhao, X., Kong, X., Huang, Z., & Bian, B. (2020). Wideband gain enhancement
263 and RCS reduction of Fabry-Perot antenna using hybrid reflection method. *IEEE Transactions on*
264 *Antennas and Propagation*, 68(9), 6497-6505. DOI: 10.1109/TAP.2020.2988949
- 265 Meriche, M. A., Attia, H., Messai, A., Mitu, S. S. I., & Denidni, T.A. (2019). Directive wideband
266 cavity antenna with single-layer meta-superstrate. *IEEE Antennas and Wireless Propagation*
267 *Letters*, 18(9), 1771-1774. DOI: 10.1109/LAWP.2019.2929579

- 268 Nguyen-Trong, N., Tran, H. H., Nguyen, T. K., & Abbosh, A. M. (2018). Wideband Fabry-Perot
269 antennas employing multilayer of closely spaced thin dielectric slabs. *IEEE Antennas and Wireless*
270 *Propagation Letters*, 17(7), 1354–1358. DOI: 10.1109/LAWP.2018.2846240
- 271 Niaz, M. W., Yin, Y., Bhatti, R. A., Cai, Y-M., & Chen, J. (2021). Wideband Fabry-Perot resonator
272 antenna employing multilayer partially reflective surface. *IEEE Transactions on Antennas and*
273 *Propagation*, 69(4), 2404–2409. DOI: 10.1109/TAP.2020.3022555
- 274 Pozar, D. M. (2011). *Microwave Engineering*, 4th ed., John Wiley & Sons Inc. ISBN: 978-0-470-
275 63155-3
- 276 Sufian, M. A., Hussain, N., Abbas, A., Lee, J., Park, S. G., & Kim, N. (2022). Mutual Coupling
277 Reduction of a Circularly Polarized MIMO Antenna Using Parasitic Elements and DGS for V2X
278 Communications. *IEEE Access*, 10, 56388–56400. DOI: 10.1109/ACCESS.2022.3177886.
- 279 Sun, Y-X., Leung, K. W., & Lu, K. (2021). Compact dual microwave/millimeter-wave planar
280 shared-aperture antenna for vehicle-to-vehicle/5G communications. *IEEE Transactions on*
281 *Vehicular Technology*, 70(5), 5071–5076. DOI: 10.1109/TVT.2021.3070353
- 282 Wang, N., Liu, Q., Wu, C., Talbi, L., Zeng, Q., & Xu, J. (2014). Wideband Fabry-Perot resonator
283 antenna with two complementary FSS layers. *IEEE Transactions on Antennas and Propagation*,
284 62(5), 2463–2471. DOI: 10.1109/TAP.2014.2308533
- 285 Wang, N., Li, J., Wei, G., Talbi, L., Zeng, Q., & Xu, J. (2015). Wideband Fabry-Perot resonator
286 antenna with two layers of dielectric superstrates. *IEEE Antennas and Wireless Propagation*
287 *Letters*, 14, 229-232. DOI: 10.1109/LAWP.2014.2360703
- 288 Wong, H., So, K. K., & Gao, X. (2016). Bandwidth enhancement of a monopolar patch antenna
289 with V-shaped slot for car-to-car and WLAN communications. *IEEE Transactions on Vehicular*
290 *Technology*, 65(3), 1130–1136. DOI: 10.1109/TVT.2015.2409886
- 291 Xing, X-Q., Lu, W-J., Ji, F-Y., Zhu, L., & Zhu, H-B. (2022). Low-profile dual-resonant wideband
292 backfire antenna for vehicle-to-everything applications. *IEEE Transactions on Vehicular*
293 *Technology*, 71(8), 8330–8340. DOI: 10.1109/TVT.2022.3175258
- 294 Zeb, B. A., Ge, Y., Esselle, K. P., Sun, Z., & Tobar, M. E. (2012). A Simple Dual-Band
295 Electromagnetic Band Gap Resonator Antenna Based on Inverted Reflection Phase Gradient.
296 *IEEE Transactions on Antennas and Propagation*, 60(10), 4522–4529. DOI:
297 10.1109/TAP.2012.2207331

20 **Abstract**

21 In this paper, a Fabry-Perot cavity (FPC) antenna with a partially reflective surface (PRS)
22 consisting of two dielectric slabs with identical thickness and permittivity to increase the gain with
23 wide bandwidth is presented. The PRS is placed in front of a broadband U-shaped microstrip patch
24 antenna to create an air-filled cavity between the PRS and the ground plane of the antenna
25 structure. The configuration of the two dielectric slabs aims to create a positive phase gradient of
26 the reflection coefficient, which strongly controls the gain bandwidth performance. The proposed
27 PRS was first designed and analyzed using a transmission line model and then verified by a full-
28 wave simulation. The measurement results show that the proposed FPC antenna achieves a gain
29 improvement of up to 5 dB compared to the antenna without PRS, with a 3-dB gain bandwidth of
30 11.5% and a broadside peak gain of 9.88 dBi. In addition, the measured impedance bandwidth is
31 approximately 18.8% and ranges from 4.95–6 GHz, which covers the required frequency band for
32 vehicle-to-everything (V2X) applications.

33 **Plain Language Summary**

34 A new design of a broadband antenna with high gain has been developed by using two identical
35 dielectric slabs placed in front of a broadband microstrip patch. This antenna is intended for
36 vehicle-to-everything (V2X) communications. The proposed configuration increases the degrees
37 of freedom and design flexibility to improve the antenna gain over a wide frequency range. The
38 proposed antenna is more practical as it is compact, lightweight, and easy to fabricate.

39 **1 Introduction**

40 The popularity of smart transportation has led to the development of vehicular wireless
41 communication systems, with vehicle-to-everything (V2X) emerging as a significant development
42 in enhancing connectivity and communication capabilities within the advancement of
43 transportation technology. In conjunction with the advanced driver assistant system (ADAS), V2X
44 will enhance safety as well as situational awareness, optimizing traffic efficiency, and overall
45 transportation effectiveness. There are two different standards for V2X communications, namely
46 the WLAN-based standard and the cellular-based standard. The WLAN-based standard refers to
47 IEEE 802.11p designed specifically for V2X communications operating in the 5 GHz band, while
48 for the cellular-based standard, e.g., cellular vehicle-to-everything (C-V2X) operating at the
49 frequency of 5.9 GHz.

50 A highly directive antenna is required to provide high antenna gain for strong signal
51 strength, a longer communication range, higher reliability, and better resistance to interference.
52 These features are essential to ensure reliable communication between vehicles and infrastructure
53 for safety enhancement. However, conventional high-gain antennas, such as reflectors, Yagi-Uda,
54 and array antennas, possess large and complex physical configurations and are thus unsuitable for
55 vehicular applications. Recently, the Fabry-Perot cavity (FPC) antennas garnered the attention of
56 many researchers due to their good characteristics, such as high efficiency, high gain, and simple
57 feeding technique. The concept of FPC antennas was first proposed in 1956 (Trentini, 1956), where
58 a PRS is placed in front of the source or feed antenna with a ground plane. The PRS is positioned
59 at a certain distance from the ground plane of the source antenna to create an air cavity in between.
60 The electromagnetic (EM) waves produced by the radiating antenna will undergo multiple
61 reflections within the cavity. This process results in an in-phase superposition of associated EM
62 waves if the resonant conditions are satisfied. Consequently, highly directive radiation is formed.

63 The conventional design of FPC has a narrow gain bandwidth (BW) because of its resonant
 64 characteristics. Several approaches have been proposed to broaden the gain BW. A single-layer
 65 unprinted dielectric substrate with a transverse permittivity gradient (TPG) was used to overcome
 66 the bandwidth limitation (Hashmi & Esselle, 2016; Baba, Hashmi, & Esselle, 2017). In Ji, Qin, &
 67 Guo (2017), by utilizing a flat ground plane at the center and angularly tilting it upwards in a
 68 trapezoid shape at the corner, the 3-dB gain bandwidth of the proposed antenna has been increased
 69 to 20.2%. These methods effectively improve the gain BW but suffer from complex design and
 70 fabrication processes. Another common technique uses a PRS with a positive phase gradient. This
 71 type of response can be obtained using a frequency-selective surface (FSS), which can be classified
 72 as a printed PRS. Two-layer PRSs consisting of hexagonal and tripod branch unit cells were
 73 employed for size reduction and to make the FPC antenna more compact, achieving a peak gain
 74 of 14.2 dBi and 3-dB gain BW of 34.2% (Guan et al., 2021). Using two types of FSS unit cells
 75 arranged in a chessboard pattern on a single-layer substrate to create a hybrid PRS (HPRS) was
 76 reported (Liu et al., 2020). The hybrid surface (HS) and reflective surface (RS) are formed by
 77 employing cross and square ring-shaped patches, which results in a measured peak gain of 17.08
 78 dBi and a 3-dB gain BW of 25.4%. A complementary unit cell design was also proposed to provide
 79 a positive phase gradient (Wang et al., 2014; Lian, Tang & Yin, 2018; Meriche et al., 2019).
 80 Subsequently, multilayer dielectric slabs, classified as unprinted PRSs, were also used to obtain a
 81 positive phase gradient (Zeb et al., 2012; Al-Tarifi et al., 2013; Wang et al., 2015). A combination
 82 of multiple thin dielectric slabs arranged closely together was reported (Nguyen-Trong et al.,
 83 2018). The thicknesses are only $0.1\lambda_{\text{subs}}$ (λ_{subs} is the dielectric wavelength at the center
 84 frequency). These slabs were separated by a $0.1\lambda_0$ (λ_0 is the free space wavelength) air gap. The
 85 measured maximum gain is 14.2 dBi, and the 3-dB gain bandwidth is up to 86%.

86 The aforementioned literature has demonstrated that the unprinted PRS exhibits superior
 87 performance in terms of gain BW enhancement despite its simple structure. Taking the potential
 88 of unprinted PRSs in gain enhancement, a broadband and high-gain FPC antenna presented in this
 89 paper is intended to work for V2X communications. The antenna configuration consists of PRSs
 90 placed over a broadband microstrip patch antenna. The proposed PRS consists of two dielectric
 91 substrate slabs with an equal thickness and dielectric constant; they are separated by an air cavity.
 92 The PRS reflection coefficient with a positive phase gradient improves gain performance over a
 93 wide frequency range.

94 The rest of this paper is organized as follows. Section 2 presents the design and analysis of
 95 the PRS. The antenna design and simulation results are illustrated in Section 3. In Section 4, the
 96 measurement results are shown, and the proposed work is compared with some competing designs
 97 in the literature. Finally, conclusions are provided in Section 5.

98 2 PRS Design and Analysis

99 A PRS is a surface that reflects part of the incident EM waves while transmitting the rest.
 100 In antenna applications, the PRS is placed in front of the feed antenna to control the radiated EM
 101 wave and improve the radiation performance of the antenna. The properties of PRSs have a strong
 102 influence on the radiation characteristics of the antenna, such as gain, radiation pattern, and
 103 operating BW. The PRS and the ground plane, which is usually part of the feed antenna, form an
 104 air cavity in which multiple reflections of EM waves occur. The mechanism for improving the
 105 antenna gain is based on the resonance of the EM waves in the cavity. The most important property
 106 of the PRS is its complex reflection coefficient ($\Gamma_{PRS} = |\Gamma_{PRS}| e^{j\phi_{PRS}}$). The reflection phase

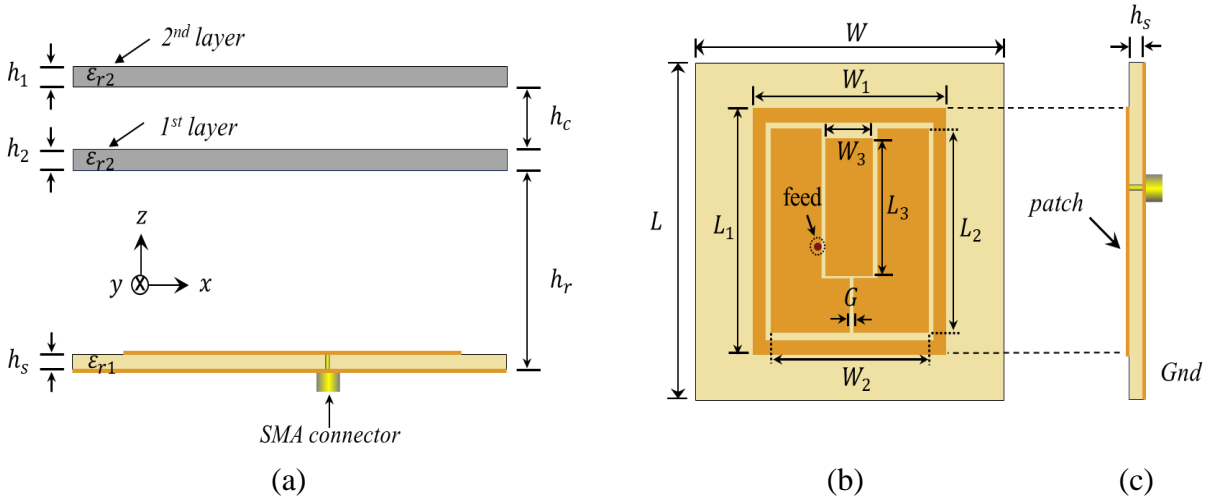


Figure 1. Design of the proposed antenna. (a) cross-section view (b) top-view of feed antenna (c) side-view of feed antenna.

107 (ϕ_{PRS}), or the phase of the reflection coefficient, of the PRS for a resonant condition of the cavity
 108 in the broadside direction of the antenna (perpendicular to the PRS) can be expressed as follows
 109 (Trentini, 1956):

$$\phi_{PRS} = \frac{4\pi h_r}{\lambda_0} + 2N\pi + \phi_{GND}, \quad (1)$$

110 where $N = 0, \pm 1, \pm 2, \dots$, ϕ_{GND} is the phase of the reflection coefficient of the ground plane, and
 111 h_r is the height of the air cavity between the PRS and the ground plane. From (1) it can be seen
 112 that a positive phase gradient of the PRS reflection coefficient over a wide frequency range is
 113 required to achieve a wide gain BW of the FPC antenna.

114 The PRS structure can consist of a variety of materials, including dielectrics, metals, or
 115 combinations thereof. One of the simplest PRS structures consists only of dielectric substrates
 116 (unprinted PRS). The functional mechanism of the PRS can be described using analytical methods
 117 such as the transmission line (TL) model. Using the TL model can show that a single-layer
 118 dielectric PRS should be half a wavelength thick to achieve the desired reflection phase
 119 characteristics (Nguyen-Trong et al., 2018). However, opting for this thickness leads to an
 120 unwieldy antenna. In addition, the desired thickness of substrate for the operating frequency range
 121 may not be commercially available.

122 The configuration of the FPC antenna presented in this work is shown in Figure 1. The
 123 proposed PRS consists of two layers of dielectric substrates with the same thickness ($h_1 = h_2$) and
 124 dielectric constant (ϵ_{r2}), separated by an air gap (h_c). The use of a two-layer PRS leads to more
 125 degrees of freedom and offers more flexibility in the design process. Several variables can be
 126 varied to achieve the desired reflection properties of the PRS, i.e., the dielectric constant and the
 127 thickness of the substrate as well as the height of the air gap. Given the unavailability of a particular
 128 material thickness in the market, modifying the air cavity height will be more convenient than
 129 altering the substrate thickness.

130 The two dielectric substrates used in the present design are Rogers RT/duroid 6010LM
 131 ($\epsilon_r = 10.2$) with a thickness of 1.9 mm ($0.11\lambda_g$), where λ_g is the wavelength in the substrate at the

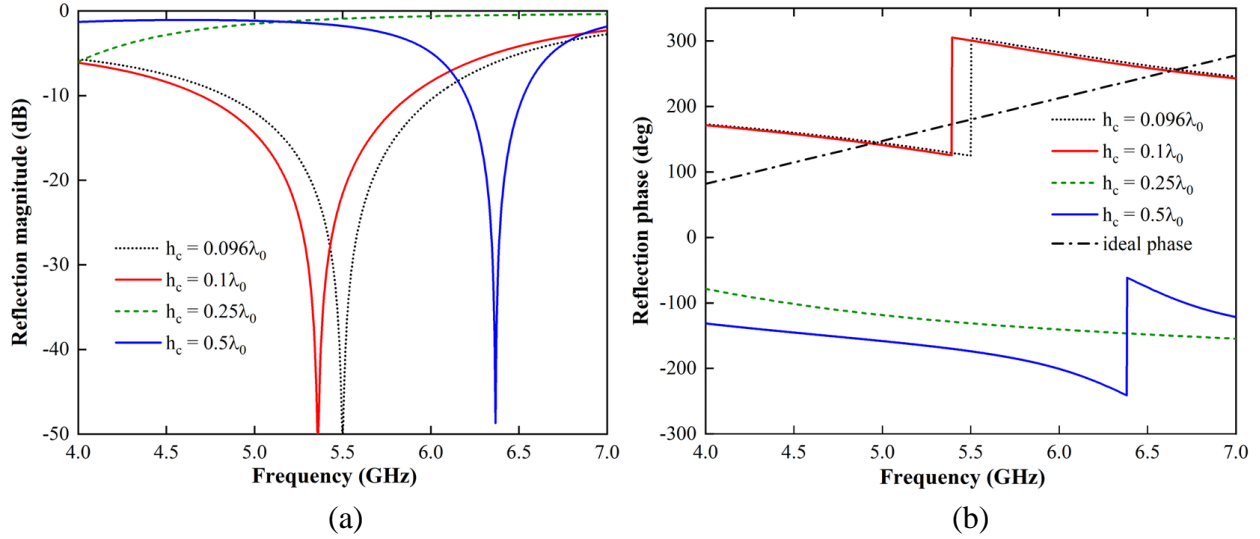


Figure 2. Reflection coefficients of the proposed PRS with different heights of the air gap calculated with the TL model. (a) magnitude (b) phase.

132 center frequency. The height of the air gap (h_c) is properly chosen to obtain a positive phase
 133 gradient. Figure 2 shows the reflection coefficients calculated with the TL model for the proposed
 134 PRS with different heights of the air gap. Also shown is a plot of the ideal positive phase gradient,
 135 which intersects with the plots of the reflection coefficient phase. It can be seen that the positive
 136 phase gradient intersects with the ideal phase at the resonant frequency when the height of the air
 137 gap is set to $0.096\lambda_0$ (5.17 mm).

138 To verify the preliminary design by the TL model, the proposed PRS structure is also
 139 simulated with CST Studio Suite (Dassault Systèmes, 2021). It is modeled as a periodic unit cell,
 140 as shown in Figure 3, to simplify the simulation. The magnitude and phase of the reflection
 141 coefficients obtained using CST Studio Suite and the TL model are compared in Figure 3. It can
 142 be seen that both results agree very well.

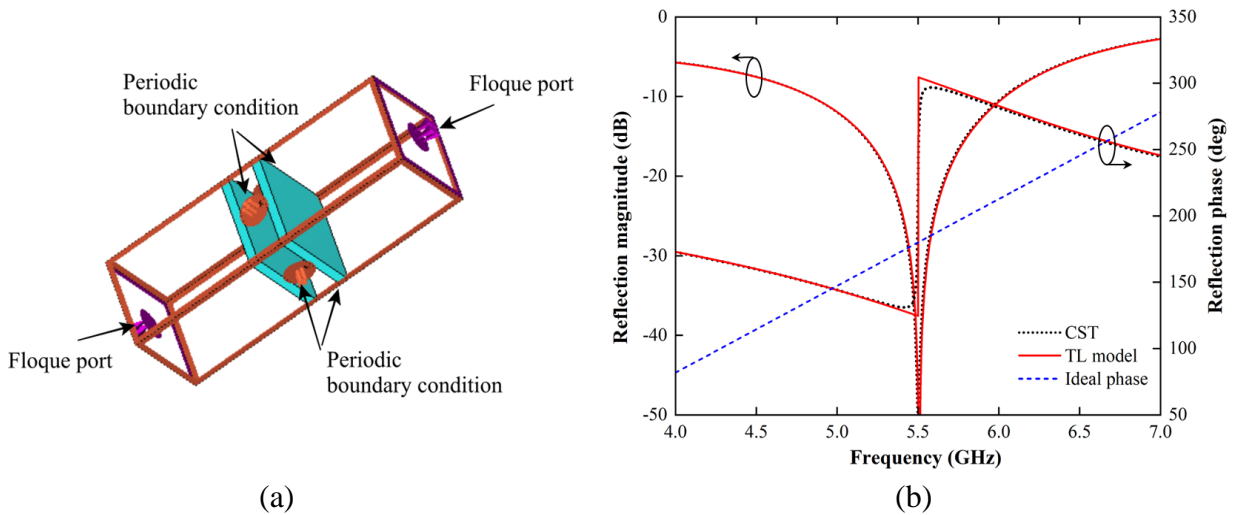


Figure 3. (a) Unit cell model of the proposed PRS in the simulation. (b) reflection coefficients of the proposed PRS determined by CST Studio Suite and the TL model.

143 It has been demonstrated in this section that by carefully choosing the thickness of the
 144 substrate and the air gap, the phase response can exhibit a positive gradient and intersect with the
 145 ideal phase given on the right-hand side (RHS) of (1) over a wide frequency band. Note that, with
 146 the proposed PRS, the positive phase gradient can be obtained with a more compact structure,
 147 namely $0.11\lambda_g + 0.095\lambda_0 + 0.11\lambda_g$.

148 3 Antenna Design and Characterization

149 The proposed FPC antenna configuration consists of two main parts: a feed antenna and
 150 the PRS. The feed antenna plays an important role in determining the performance of the designed
 151 antenna. The directivity of the feed antenna contributes to the achieved directivity of the FPC
 152 antenna as described by the following equation (Niaz et al., 2021):

$$D_{FPCA} = D_{feed} + D_{PRS}, \quad (2)$$

153 where D_{FPCA} is the directivity of FPC antenna, D_{feed} and D_{PRS} are the feed antenna and PRS
 154 directivities, respectively.

155 In this paper, the microstrip patch antenna is used as the feed antenna because it is known
 156 for its outstanding features such as low cost, low profile, planar structure, and easy fabrication.
 157 The microstrip patch antenna is printed on the FR-4 substrate ($\epsilon_{r1} = 4.3$) with a thickness (h_s) of
 158 1.6 mm. The 50-ohm coaxial probe is used to feed the antenna through the SMA connector. The
 159 design evolution of the microstrip antenna and their simulated reflection coefficient magnitude
 160 ($|S_{11}|$) results are given in Figure 4.

161 Note that Ant_1 consists of a U-shaped patch to obtain a wide impedance BW ($|S_{11}| \leq -10$
 162 dB). This antenna generates two resonant modes, namely TM_{20} (5 GHz) and TM_{21} (5.9 GHz). The
 163 introduction of a slot into the structure (Ant_2) causes the second resonance TM_{02} (5.7 GHz) to
 164 appear and is combined with a rectangular patch (Ant_3) placed in the center of the U-shaped
 165 patch. This configuration creates a multimode resonance, resulting in a wide impedance BW.
 166 Finally, Ant_4 is designed by adding the rectangular ring to further broaden the impedance BW.
 167 The final design of the microstrip antenna exhibits an impedance BW range from 4.969 to 6.001
 168 GHz (18.96%), aligning perfectly with the frequency band requirements for V2X applications.

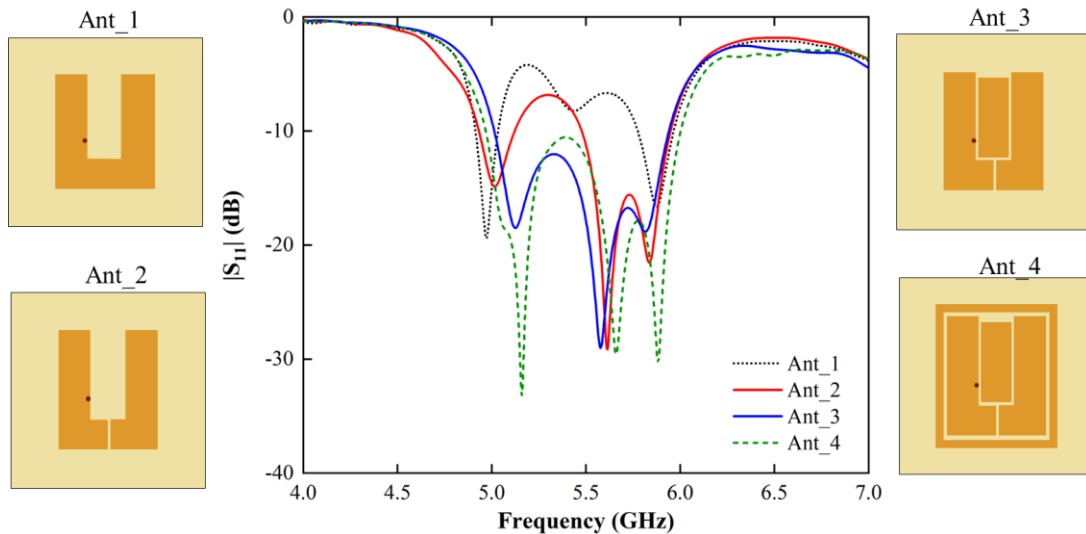


Figure 4. Geometry evolution of the microstrip antenna and its simulated $|S_{11}|$.

169 The designed PRS is then integrated into the feed antenna. The FPC is formed by the PRS
 170 and the ground plane of the feed antenna. The reflection phase of PRS is known from the
 171 simulation results, and the reflection coefficient of the ground plane (assuming PEC) is
 172 approximately -1 . Therefore, the height of the FPC between the PRS and the ground plane (h_r)
 173 can be determined using (1). With $\phi_{PRS} = 221.76^\circ$, $\phi_{GND} \approx 180^\circ$, and $N = 0$, $h_r = 30.44$ mm is
 174 obtained. However, to enhance the gain performance of the FPC antenna, the cavity height (h_r)
 175 was further optimized using CST Studio. Figure 5 shows the $|S_{11}|$ and broadside gain characteristics
 176 when h_r is varied. After the optimization, it is found that $h_r = 28.67$ mm is the optimum value.
 177 The geometric parameters of the proposed FPC antenna are listed in Table 1.

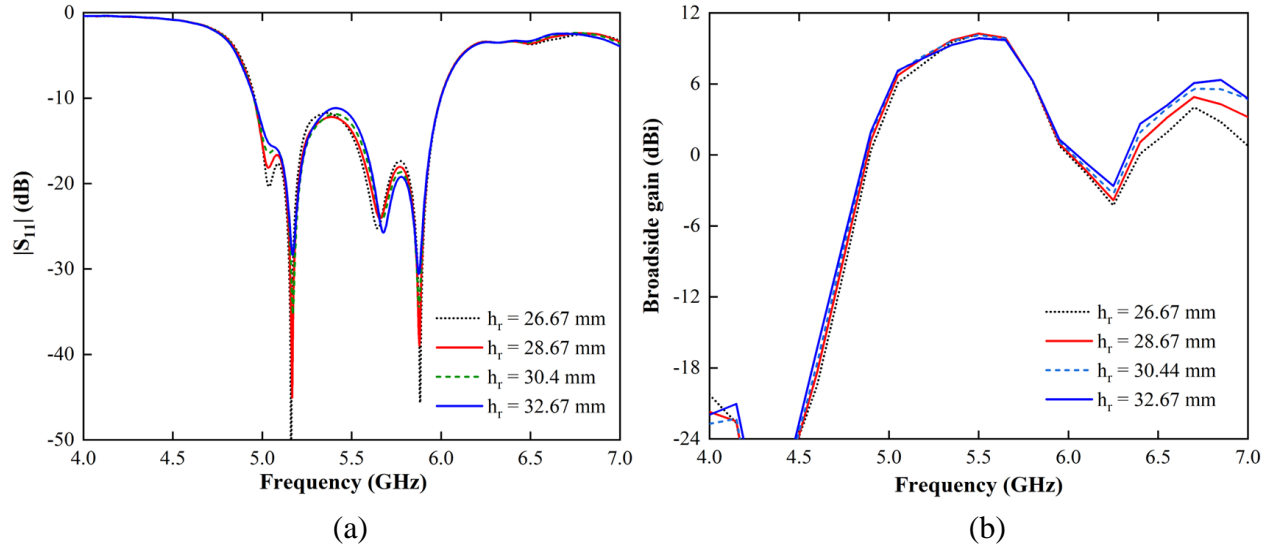


Figure 5. Performances of the proposed antenna with values of h_r varied. (a) simulated $|S_{11}|$ (b) simulated broadside gain.

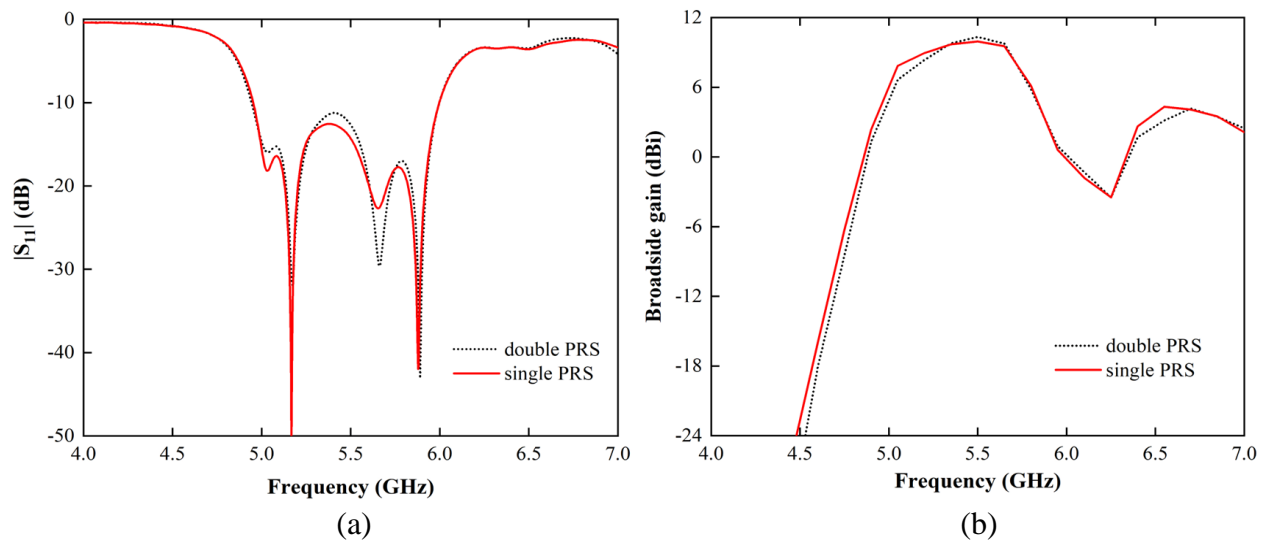


Figure 6. Comparison of the proposed antenna with single-layer PRS. (a) simulated $|S_{11}|$ (b) simulated broadside gain.

179

Table 1 Geometric Parameters of The Proposed FPC Antenna.

| Parameters | Values (mm) | Parameters | Values (mm) | Parameters | Values (mm) |
|------------|-------------|------------|-------------|------------|-------------|
| L | 60 | W_2 | 25 | h_1 | 1.9 |
| W | 60 | L_3 | 19.5 | h_2 | 1.9 |
| L_1 | 36 | W_3 | 8 | h_r | 28.67 |
| W_1 | 32 | G | 1 | h_c | 5.17 |
| L_2 | 28 | h_s | 1.6 | — | — |

180

181

182

183

184

A half-wavelength thickness of single-layer PRS is compared with the proposed double-layer PRS. The single-layer PRS has a thickness of 8.5 mm, whilst the proposed double-layer PRS has an overall thickness of 8.8 mm (including air gap). The thicknesses are almost equal. However, the proposed PRS is lighter. As seen, the performances of simulated $|S_{11}|$ and broadside gain are very similar to each other as plotted in Figure 6.

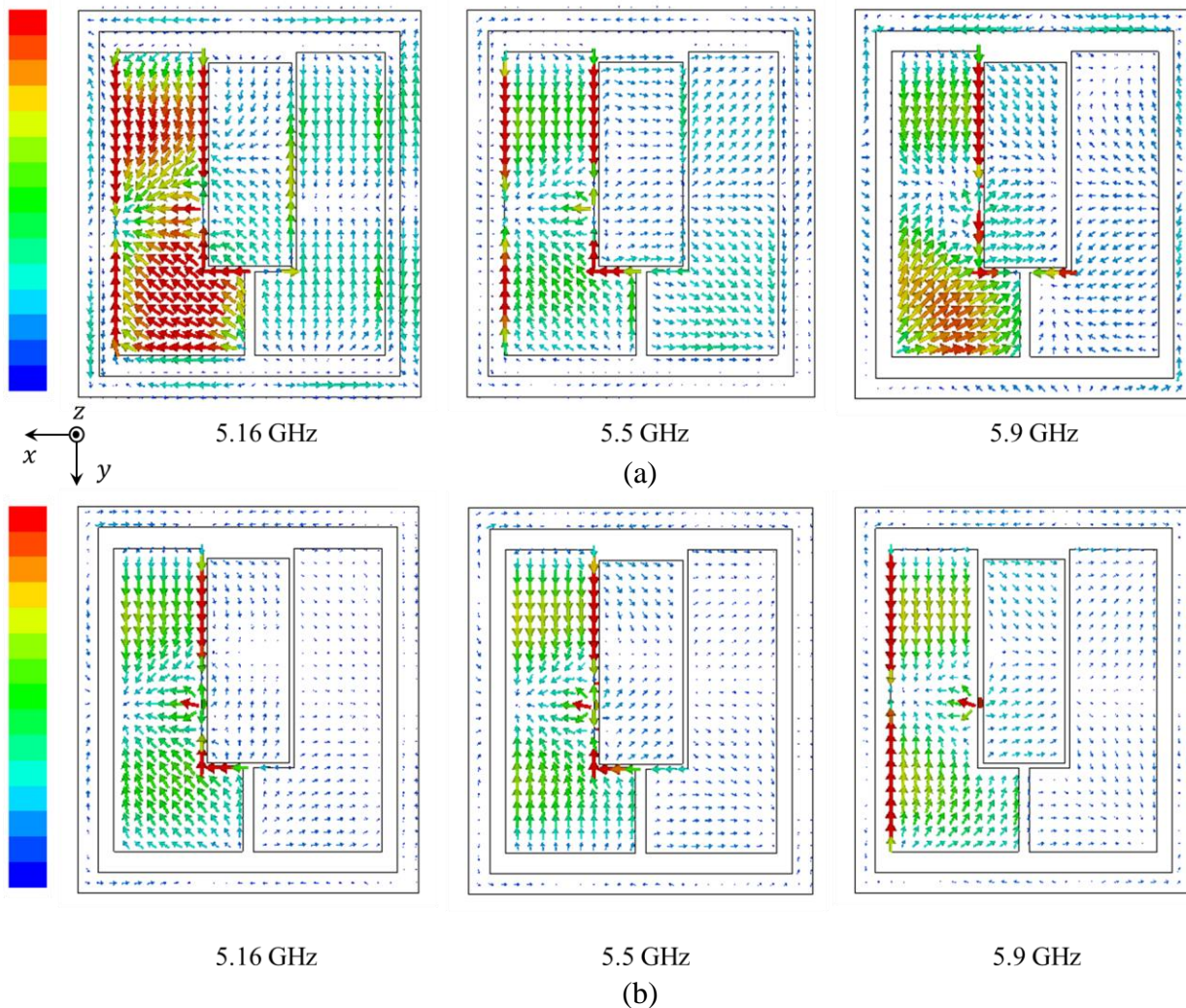


Figure 7. Surface current distribution at three resonant frequencies. (a) feed antenna (without the PRS) (b) feed antenna with the PRS.

185 Figure 7 shows the surface current distribution on the metallic portion of the antenna at
 186 three resonant frequencies. The introduction of the PRS in the feed antenna significantly affects
 187 the current distribution. The PRS can alter the EM environment around the antenna, leading to
 188 changes in the way current flows on the antenna structure. The reflective properties of the PRS
 189 affect the phase and amplitude of the EM waves, which in turn, can impact the impedance
 190 matching, radiation pattern, and overall performance of the feed antenna.

191 4 Results and Discussions

192 To validate the simulation results, the proposed FPC antenna is then fabricated where the
 193 prototype is given in Figure 8(a). The nylon is used to support the PRS layers and create an air
 194 cavity. The measurements were performed in an anechoic chamber as shown in Figure 8(b).

195 The comparison of simulated and measured $|S_{11}|$ is depicted in Figure 9(a), where the -10
 196 dB impedance BW for the feed antenna (without the PRS) is 18.82% (4.969–6.001 GHz), and
 197 18.64% (4.963–5.983 GHz) with respect to the center frequency, respectively. Additionally, it can
 198 be seen that the simulated -10 dB impedance BW for the antenna with PRS is 19.02%
 199 (4.954–5.995 GHz), and the measured one is 18.80% (4.95–5.977 GHz). In Figure 9(b), the
 200 presence of PRS significantly increases the broadside gain of the feed antenna from 4.85 to 9.88
 201 dBi, with a 3-dB gain BW of 11.5% in the measured result, while the simulated result is from 5.89
 202 to 10.32 dBi with 11.74% of 3-dB gain BW. Overall, the simulated and measured results are in
 203 good agreement. The slight discrepancies may be caused by fabrication errors, uncertainty of
 204 material properties, and soldering issues.

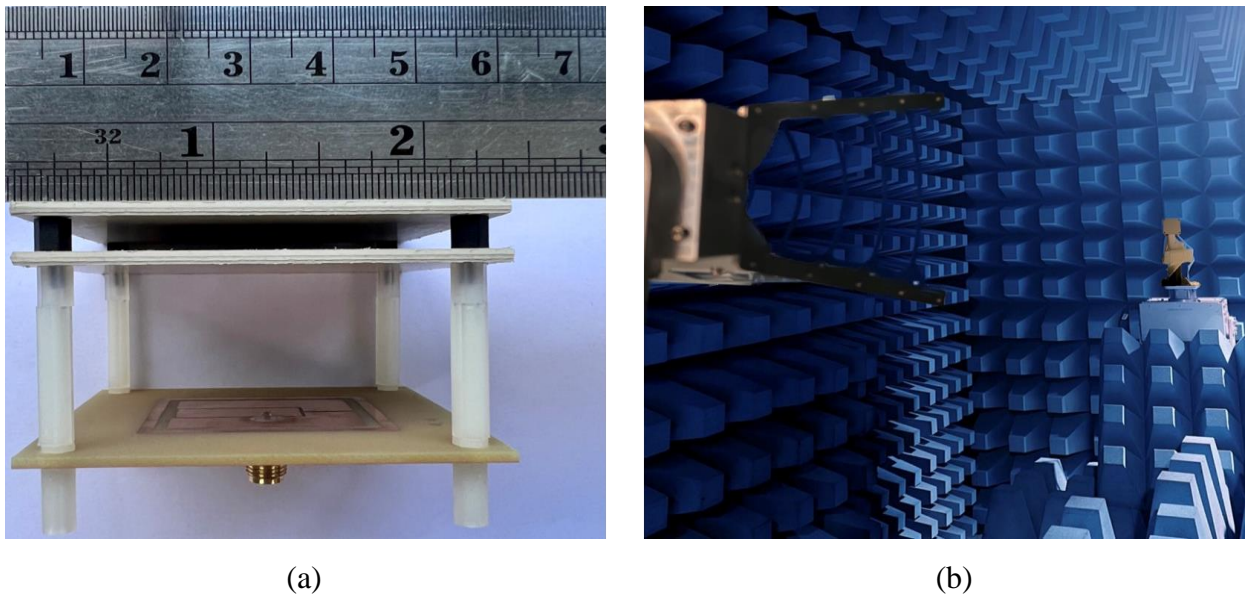


Figure 8. (a) Fabricated FPC antenna (b) radiation measurement set-up.

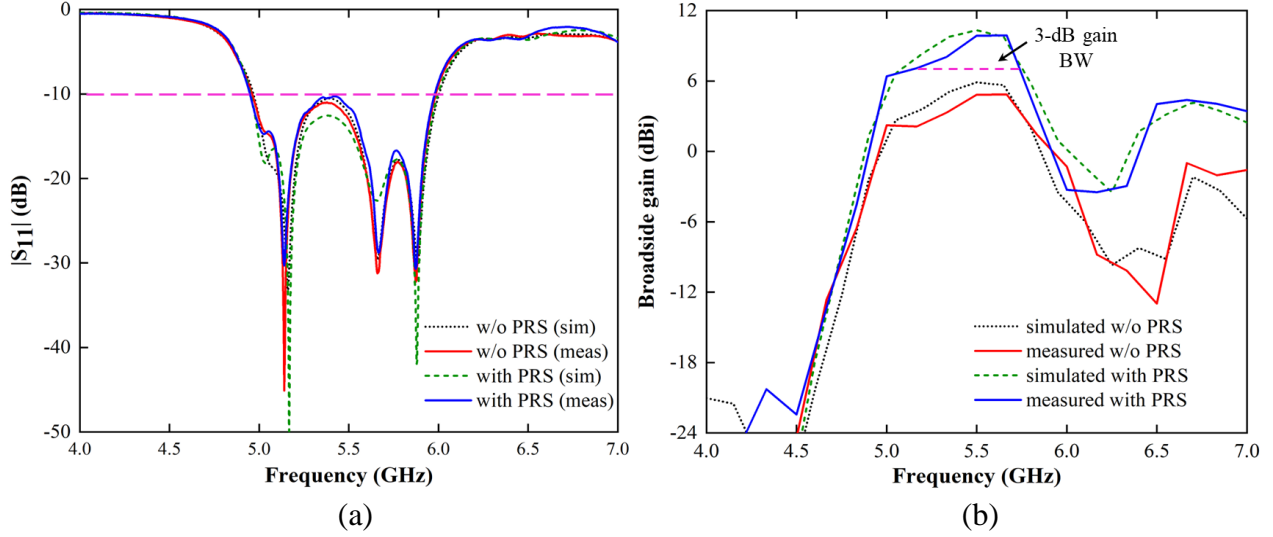


Figure 9. The comparison between simulated and measured results of the FPC antenna. (a) $|S_{11}|$ (b) broadside gain.

206 The simulated and measured radiation patterns of the proposed antenna at 5.16, 5.5, and
 207 5.9 GHz are plotted in Figure 10. It can be observed that the main beam orientation of the FPC
 208 antenna is in the broadside direction at three distinct frequencies in the H-plane, while at 5.9 GHz
 209 the main beam orientation is slightly tilted in the E-plane. It is noteworthy that since the antenna
 210 excitation is not symmetric in the E- and H-planes, the antenna has an asymmetric radiation
 211 pattern in both planes.

212 Table 2 compares the performance of the proposed FPC antenna with some previous works
 213 of vehicular antennas in the literature. It can be seen that the proposed antenna has a comparatively
 214 high gain and a fairly wide BW with a relatively compact size. It also has a simple structure with
 215 only a single feed and is easy to fabricate.

216 **Table 2** Comparison between the Proposed FPC Antenna and Reported Antennas.
 217

| References | f_{min} (GHz) | Size ($\lambda_{f_{min}}$ *) | IBW (%) | Max. gain (dBi) | 3-dB gain BW (%) | Num. of layers | Rad. pattern type |
|--------------------------|-----------------|--|--------------|-----------------|------------------|----------------|-------------------|
| (Sufian et al., 2022) | 5.61 | $1.38 \times 1.38 \times 0.03$ | 7.05 | 7.68 | N/A | 1 | Directional |
| (Xing et al., 2022) | 4.82 | $3.2 \times 2.41 \times 0.08$ | 27.6 | 4.2 | 7.8 | 1 | Directional |
| (Sun, Leung, & Lu, 2021) | 5.3 | $0.53 \times 0.35 \times 0.11$ | 41.6 | 8.46 | 10.3 | 2 | Directional |
| (Gao et al., 2018) | 5.42 | $3.07 \times 3.07 \times 0.08$ | 9.8 | 7.5 | N/A | 2 | Omni-directional |
| (Wong, So & Gao, 2016) | 4.82 | $1.03 \times 1.03 \times 0.05$ | 32.2 | 6.5 | 32.25 | 1 | Omni-directional |
| This work | 4.95 | $0.99 \times 0.99 \times 0.62$ | 18.80 | 9.88 | 11.5 | 3 | Directional |

218 * $\lambda_{f_{min}}$ is the free-space wavelength at the lowest frequency of the bandwidth.

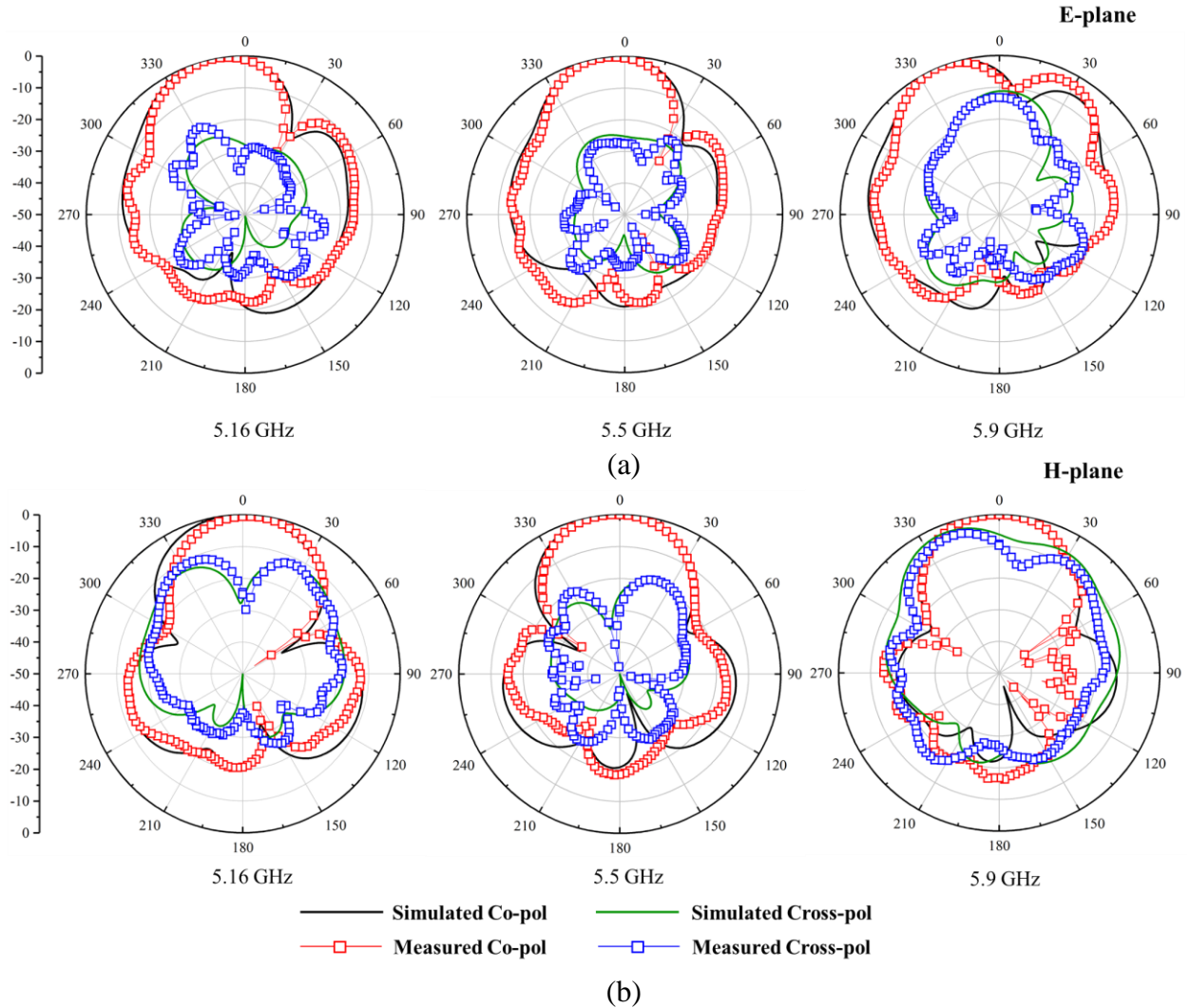


Figure 10. Simulated and measured radiation patterns of the FPC antenna at 5.16 GHz, 5.5 GHz, and 5.9 GHz. (a) E-plane (b) H-plane.

219 5 Conclusions

220 This paper presents a broadband high-gain FPC antenna for V2X communications. The
 221 gain-bandwidth performance is achieved through the appropriate design of the PRS reflection
 222 coefficient that exhibits a positive phase gradient. The proposed PRS is readily realized by two
 223 dielectric substrates with the same dielectric constant and thickness separated by an air gap with a
 224 suitable height. This structure is relatively practical since it is compact, lightweight, and easy to
 225 fabricate. The measurement results show that the proposed PRS can effectively increase the gain
 226 of the feed antenna with wide gain BW. In addition, a novel asymmetric PRS design based on
 227 compact microstrip resonant cells (CMRCs) is currently investigated for future works.
 228 Experimental characterizations of this novel PRS design are still in progress, where the
 229 measurement results will be reported later.

231 **Acknowledgments**

232 This research was funded in parts by (i) Ratchadapisek Somphot Fund for Wireless
233 Network & Future Internet Research Unit, Chulalongkorn University [Contract no. GRU
234 6409521015-1], (ii) National Science, Research and Innovation Fund (NSRF), King Mongkut's
235 University of Technology North Bangkok [Project no. KMUTNB-FF-67-A-04], and (iii) The
236 Ministry of Science and Technology, Taiwan.

237

238 **References**

- 239 Al-Tarifi, M. A., Anagnostou, D. E., Amert, A. K., & Whites, K. W. (2013). Bandwidth
240 enhancement of the resonant cavity antenna by using two dielectric superstrates. *IEEE*
241 *Transactions on Antennas and Propagation*, 61(4), 1898-1908. DOI: 10.1109/TAP.2012.2231931
- 242 Baba, A. A., Hasmi, R. M., & Esselle, K. P. (2017). Achieving a large gain-bandwidth product
243 from a compact antenna. *IEEE Transactions on Antennas and Propagation*, 65(7), 3437–3446.
244 DOI: 10.1109/TAP.2017.2700016
- 245 Dassault Systèmes. (2021). *CST Studio Suite 2021, Dassault Systèmes*. Retrieved from:
246 <https://www.3ds.com/products-services/simulia/products/cst-studio-suite/solvers/>
- 247 Gao, S., Ge, L., Zhang, D., & Qin, W. (2018). Low-profile dual-band stacked microstrip
248 monopolar patch antenna for WLAN and car-to-car communications. *IEEE Access*, 6,
249 69575–69581. DOI: 10.1109/ACCESS.2018.2877420
- 250 Guan, Y., Jiao, Y-C., Yan, Y-D., Feng, Y., Weng, Z., & Tian, J. (2021). Wideband and compact
251 Fabry–Perot resonator Antenna using partially reflective surfaces with regular hexagonal unit.
252 *IEEE Antennas and Wireless Propagation Letters*, 20(6), 1048-1052. DOI:
253 10.1109/LAWP.2021.3070376
- 254 Hashmi, R. M., & Esselle, K. P. (2016). A class of extremely wideband resonant cavity antennas
255 with large directivity-bandwidth products. *IEEE Transactions on Antennas and Propagation*,
256 64(2), 830–835. DOI: 10.1109/TAP.2015.2511801
- 257 Ji, L-Y., Qin, P-Y., & Guo, Y. J. (2018). Wideband Fabry-Perot cavity antenna with a shaped
258 ground plane. *IEEE Access*. 6. 2291–2297. DOI: 10.1109/ACCESS.2017.2782749
- 259 Lian, R., Tang, Z., & Yin, Y. (2018). Design of a broadband polarization-reconfigurable Fabry-
260 Perot resonator antenna. *IEEE Antennas and Wireless Propagation Letters*, 17(1), 122–125. DOI:
261 10.1109/LAWP.2017.2777502
- 262 Liu, Z., Liu, S., Zhao, X., Kong, X., Huang, Z., & Bian, B. (2020). Wideband gain enhancement
263 and RCS reduction of Fabry-Perot antenna using hybrid reflection method. *IEEE Transactions on*
264 *Antennas and Propagation*, 68(9), 6497–6505. DOI: 10.1109/TAP.2020.2988949
- 265 Meriche, M. A., Attia, H., Messai, A., Mitu, S. S. I., & Denidni, T.A. (2019). Directive wideband
266 cavity antenna with single-layer meta-superstrate. *IEEE Antennas and Wireless Propagation*
267 *Letters*, 18(9), 1771–1774. DOI: 10.1109/LAWP.2019.2929579

- 268 Nguyen-Trong, N., Tran, H. H., Nguyen, T. K., & Abbosh, A. M. (2018). Wideband Fabry-Perot
269 antennas employing multilayer of closely spaced thin dielectric slabs. *IEEE Antennas and Wireless*
270 *Propagation Letters*, 17(7), 1354–1358. DOI: 10.1109/LAWP.2018.2846240
- 271 Niaz, M. W., Yin, Y., Bhatti, R. A., Cai, Y-M., & Chen, J. (2021). Wideband Fabry-Perot resonator
272 antenna employing multilayer partially reflective surface. *IEEE Transactions on Antennas and*
273 *Propagation*, 69(4), 2404–2409. DOI: 10.1109/TAP.2020.3022555
- 274 Pozar, D. M. (2011). *Microwave Engineering*, 4th ed., John Wiley & Sons Inc. ISBN: 978-0-470-
275 63155-3
- 276 Sufian, M. A., Hussain, N., Abbas, A., Lee, J., Park, S. G., & Kim, N. (2022). Mutual Coupling
277 Reduction of a Circularly Polarized MIMO Antenna Using Parasitic Elements and DGS for V2X
278 Communications. *IEEE Access*, 10, 56388–56400. DOI: 10.1109/ACCESS.2022.3177886.
- 279 Sun, Y-X., Leung, K. W., & Lu, K. (2021). Compact dual microwave/millimeter-wave planar
280 shared-aperture antenna for vehicle-to-vehicle/5G communications. *IEEE Transactions on*
281 *Vehicular Technology*, 70(5), 5071–5076. DOI: 10.1109/TVT.2021.3070353
- 282 Wang, N., Liu, Q., Wu, C., Talbi, L., Zeng, Q., & Xu, J. (2014). Wideband Fabry-Perot resonator
283 antenna with two complementary FSS layers. *IEEE Transactions on Antennas and Propagation*,
284 62(5), 2463–2471. DOI: 10.1109/TAP.2014.2308533
- 285 Wang, N., Li, J., Wei, G., Talbi, L., Zeng, Q., & Xu, J. (2015). Wideband Fabry-Perot resonator
286 antenna with two layers of dielectric superstrates. *IEEE Antennas and Wireless Propagation*
287 *Letters*, 14, 229-232. DOI: 10.1109/LAWP.2014.2360703
- 288 Wong, H., So, K. K., & Gao, X. (2016). Bandwidth enhancement of a monopolar patch antenna
289 with V-shaped slot for car-to-car and WLAN communications. *IEEE Transactions on Vehicular*
290 *Technology*, 65(3), 1130–1136. DOI: 10.1109/TVT.2015.2409886
- 291 Xing, X-Q., Lu, W-J., Ji, F-Y., Zhu, L., & Zhu, H-B. (2022). Low-profile dual-resonant wideband
292 backfire antenna for vehicle-to-everything applications. *IEEE Transactions on Vehicular*
293 *Technology*, 71(8), 8330–8340. DOI: 10.1109/TVT.2022.3175258
- 294 Zeb, B. A., Ge, Y., Esselle, K. P., Sun, Z., & Tobar, M. E. (2012). A Simple Dual-Band
295 Electromagnetic Band Gap Resonator Antenna Based on Inverted Reflection Phase Gradient.
296 *IEEE Transactions on Antennas and Propagation*, 60(10), 4522–4529. DOI:
297 10.1109/TAP.2012.2207331